Rapid Communications

Spatiotemporal correlation uncovers characteristic lengths in cardiac tissue

Alessandro Loppini,[1] Alessio Gizzi,[1,*] Christian Cherubini,[1,2] Elizabeth M. Cherry,[3] Flavio H. Fenton,[4] and Simonetta Filippi[1,2]

[1]*Department of Engineering, Campus Bio-Medico University of Rome, Via A. del Portillo 21, I-00128 Rome, Italy*
[2]*ICRANet, Piazza delle Repubblica 10, I-65122 Pescara, Italy*
[3]*School of Mathematical Sciences, Rochester Institute of Technology, 85 Lomb Memorial Drive, Rochester, New York 14623, USA*
[4]*School of Physics, Georgia Institute of Technology, 837 State Street, Atlanta, Georgia 30332, USA*

(Received 14 June 2018; revised manuscript received 5 June 2019; published 16 August 2019)

Complex spatiotemporal patterns of action potential duration have been shown to occur in many mammalian hearts due to period-doubling bifurcations that develop with increasing frequency of stimulation. Here, through high-resolution optical mapping experiments and mathematical modeling, we introduce a characteristic spatial length of cardiac activity in canine ventricular wedges via a spatiotemporal correlation analysis, at different stimulation frequencies and during fibrillation. We show that the characteristic length ranges from 40 to 20 cm during one-to-one responses and it decreases to a specific value of about 3 cm at the transition from period-doubling bifurcation to fibrillation. We further show that during fibrillation, the characteristic length is about 1 cm. Another significant outcome of our analysis is the finding of a constitutive phenomenological law obtained from a nonlinear fitting of experimental data which relates the conduction velocity restitution curve with the characteristic length of the system. The fractional exponent of $3/2$ in our phenomenological law is in agreement with the domain size remapping required to reproduce experimental fibrillation dynamics within a realistic cardiac domain via accurate mathematical models.

DOI: 10.1103/PhysRevE.100.020201

Exploiting characteristic lengths and times represents a primary strategy to understand natural phenomena. In this perspective, heart dynamics shows multiple spatial and temporal scales ranging from physiological up to pathological regimes [1–3]. Complex series of cardiac spatiotemporal activation patterns, e.g., phase-locking and period-doubling bifurcations [4–6], can lead to a disorganized ventricular electrical activity—fibrillation (see Fig. 1 for an experimental example of the induction of fibrillation)—classified as life-threatening cardiac arrhythmias in the clinical community. These phenomena are known to be supported by specific physical indicators, e.g., spatial dispersion of repolarization [7–9] and associated abnormal values of action potential (AP) duration and conduction velocity (CV), producing oscillations in the electrocardiogram signal and suggesting their clinical importance in risk stratification for sudden cardiac death [10]. Attempts to classify different regimes involved in cardiac activity dates back to Wiggers [11], and this subject is still widely studied in animal experiments and isolated myocardium as well as supported by sophisticated mathematical models [12–17]. Indicators quantifying general properties of ventricular fibrillation have been proposed in the physics literature [18–21], e.g., order parameters and correlation functions. However, a comprehensive spatiotemporal index, able to characterize the different regimes, is still missing, thus limiting our predictive power.

In this Rapid Communication, we provide an experimental-modeling rationale identifying a predictive indicator of cardiac dynamics. We make use of AP optical mapping recordings on endocardial canine ventricular wedges [we refer to Gizzi *et al.* [5] and the Supplemental Material (SM) [22] for details on the experimental protocol] and fine-tuned phenomenological mathematical models of cardiac electrical activity [9,23] measuring characteristic lengths under different dynamical regimes. We unveil constitutive properties of the heart, further identifying a normalized characteristic length which may serve as a predictive indicator of period-doubling bifurcations (alternans). We explain such observations by introducing a phenomenological relation linking characteristic length and conduction velocity. Strikingly, such a constitutive law allows us to accurately predict and reproduce spatiotemporal fibrillation behaviors by applying a domain size mapping. This methodology prevents any additional model tuning, which usually represents a necessary extra step to simulate arrhythmias in realistic cardiac geometries.

Mathematical model tuning. We make use of a monodomain formulation of the four-variable minimal model for cardiac electrophysiology [23] fine tuned upon experimental data (see SM). The objective here is to highlight the complex multiscale nature of the cardiac tissue and the intrinsic coupling between its spatial and temporal features. In this perspective, Fig. 2(a) compares the time course of two consecutive action potentials during fast electrical pacing [cycle length (CL)] quantifying the action potential duration (APD) for a representative example of canine optical mapping recordings [5] and one-dimensional (1D) simulations. Figure 2(b) compares the conduction velocity (CV) calculated on the two-dimensional (2D) endocardial surface (average and standard error from seven samples—squared symbols)

*a.gizzi@unicampus.it

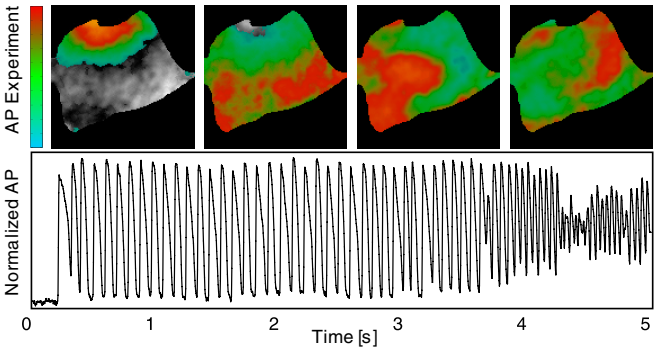

FIG. 1. Endocardial action potential (AP) voltage data from fluorescence optical mapping showing the transition from normal rhythm to ventricular tachycardia up to ventricular fibrillation. Spatial distribution at selected frames (top) and time course of a single pixel (bottom). In sequence: Top-down propagating front, top-down wave back, single clockwise spiral, double-clockwise spirals. The color code refers to normalized voltage amplitude. The grayscale background represents the endocardial ventricular tissue [5].

for decreasing values of CL (restitution protocol [24]) with respect to 1D model prediction (solid line). Figure 2(c) shows experimental and simulated endocardial electrical excitations during a single action potential wave propagation, confirming the accuracy of the numerical wave-front dynamics. In this case, the phase field approach is adopted [25] such that the computational domain size corresponds to the irregular optical area taken from the measures. As an additional level of information, isochrones of activation are provided in both cases to highlight further the need for nontrivial anisotropies in the computational model to reproduce the observed dynamics [26]. Finally, Fig. 2(d) shows a spatial view of alternans maps on the optical field of view obtained on the same tissue for different CL. In particular, from left to right, CL decreases, thus inducing a higher and more heterogeneous distribution of alternans in the tissue, up to 25 ms of APD difference for two consecutive beats. We assume the presence of alternans when the condition $|\Delta\mathrm{APD}| > 2$ ms is fulfilled [5] (see details in SM).

Correlation measure. We introduce a quantitative analysis of fluorescence optical mapping signals based on the calculation of correlation functions and the identification of the corresponding characteristic spatial length (decay length L_0). Specifically, we computed a two-point operator within a square box extracted from the mapped tissue [see Fig. 2(d)],

$$R(\vec{x},\vec{r}) = \frac{\langle (V_A - \langle V_A\rangle_t)(V_B - \langle V_B\rangle_t)\rangle_t}{\sigma_A \sigma_B}, \qquad (1)$$

where $V_A = V(\vec{x},t)$, $V_B = V(\vec{x}+\vec{r},t)$, $\langle\cdot\rangle_t$ represents the time average computed over a selected time window, and σ_A, σ_B are the standard deviations of V_A and V_B, respectively. We finally average $R(\vec{x},\vec{r})$ over the whole squared domain to compute the global correlation index at distance $\vec{r}$ defining the characteristic length L_0 as $R(\vec{r}) \propto \exp(-|\vec{r}|/L_0)$ (see details in SM).

Evaluated L_0 values are shown in Fig. 3(a) for seven different ventricular preparations. Optical data (squared symbols) are characterized by an average L_0 decreasing from 38 to

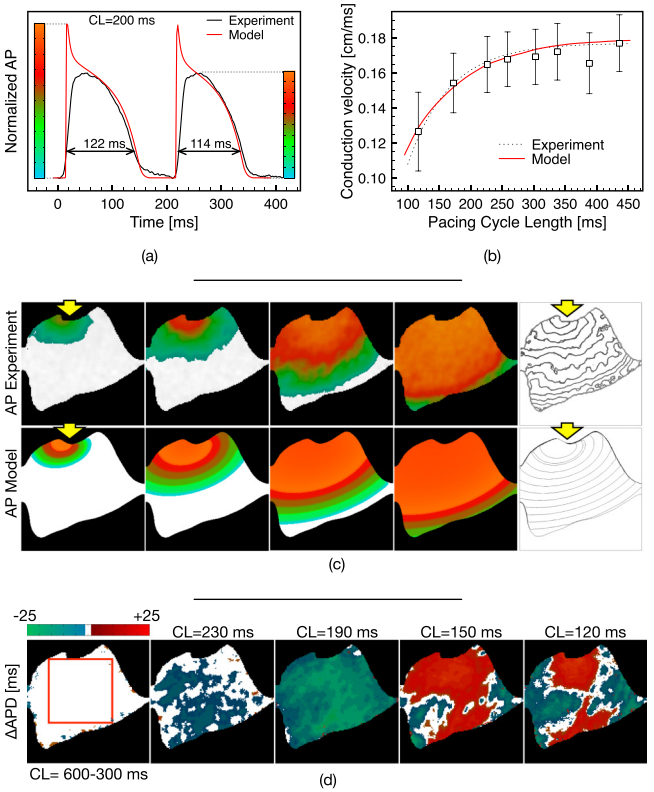

FIG. 2. (a) Experimental (black) and simulated (red–light gray) AP time course for two consecutive activations during fast pacing with the indication of APD alternans. (b) Conduction velocity restitution curve (mean and standard error) for experimental tissue samples (symbol), fitting exponential law (dashed), and one-dimensional model prediction (solid). (c) Representative endocardial wave-front propagations and corresponding isochrones from experiments (top) and model (bottom). Arrows indicate the location of the pacing electrode. (d) Spatial map of ΔAPD alternans evolution during pace-down stimulation protocol [5]: nonalternating (white), concordant (blue–singly gray), discordant alternans (blue/red–multigray). The red square (left) indicates the region selected to compute the correlation function.

3 cm for the endocardial surface (34 to 4 cm for the epicardial surface—not shown), reducing CL from 450 to 115 ms. As expected, we observe tissue variability, but it decreases at short CLs where smaller L_0 values are identified, and significant exponential decay of the two-point correlation function is obtained. The robustness of the methodology is further confirmed by two-dimensional numerical simulations [solid circle symbols in Fig. 3(a)] that match the experimental decay length trend finally merging the mean experimental value at short CLs.

We further characterize the multiple transitions occurring at fast pacing enriching the previous analysis with the measure of the normalized decay length L^* in Fig. 3(b),

$$\langle L_0\rangle = \frac{L_0^+ + L_0^-}{2}, \quad L^* = \frac{L_0^+ - \langle L_0\rangle}{\langle L_0\rangle}, \qquad (2)$$

representing an integral quantification of the well-known cardiac beat-to-beat variability. In particular, we identify (i) the transition from no alternans to concordant alternans, when a

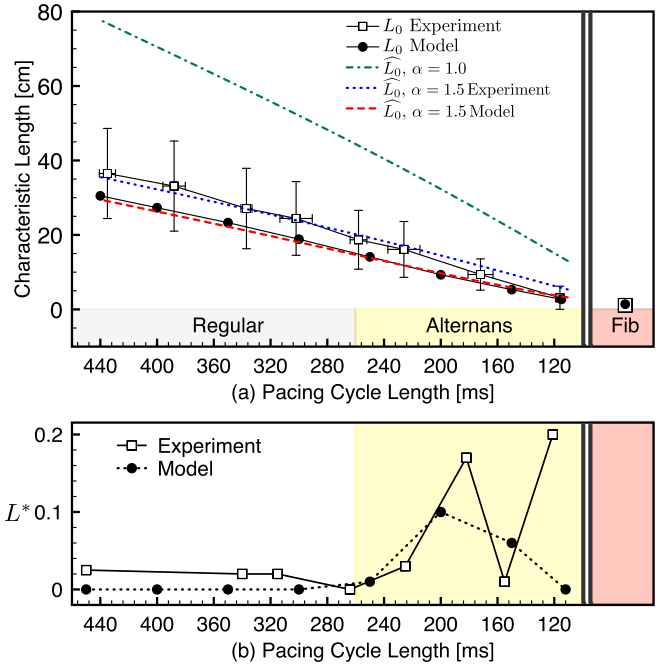

FIG. 3. (a) Decay length as a function of pacing cycle length for endocardial experimental recordings and corresponding model simulations. Standard deviation is superimposed to the experimental measures. Dashed curves indicate the fitted estimate of characteristic length $\widehat{L_0}$, Eq. (3), in the linear case ($\alpha = 1$) and fitted for experiments and model ($\alpha = 1.5$). (b) Normalized decay length L^* vs pacing cycle length for a representative experimental recording (solid) and model (dashed).

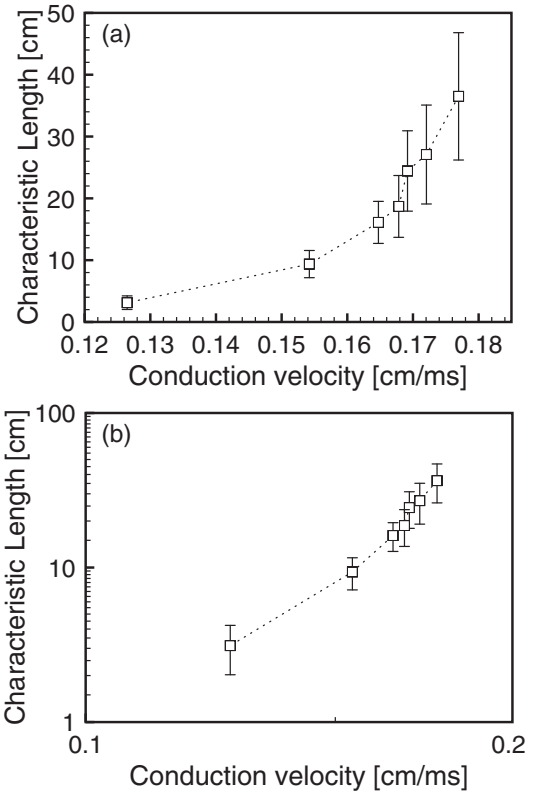

FIG. 4. Characteristic length vs CV in (a) linear and (b) log-log scales. Squares denote experimental measures at specific cycle lengths. Vertical bars denote standard deviation.

net increase of L^* is observed, and (ii) the transition from concordant alternans to discordant alternans when consecutive CL-dependent oscillations of L^* are present. We also note that L^* is not null for the experimental data at slow pacing rates (CL $>$ 300 ms), thus implying an intrinsic dispersion in the tissue, and L^* oscillates by lowering CL within the discordant alternans regime (CL $<$ 150 ms). Interestingly, an intermediate *resynchronization* pattern appears, $L^* \simeq 0$, observed only as a critical state before a transition occurs. We justify such transitions in terms of L^* values obtained via numerical simulation [dashed line in Fig. 3(b)]. The model can reproduce the normalized decay length patterns both in amplitude and timing, in particular predicting the onset of alternans. However, it does not capture either dispersion at slow pacing rates nor multiple oscillations at fast CLs. We stress here that these two limitations are common in the current literature of computational cardiology [27]. An effort in introducing memory in time and dispersion in space [17,26] aims, in fact, at reproducing *in silico* arrhythmic scenarios that usually require nonphysical (larger) simulation domains and *ad hoc* parameters' choice.

Phenomenological constitutive theory. We assume that the excitation wave velocity varies with the pacing period according to the exponential law $\mathrm{CV(CL)} = A - B\exp(C\,\mathrm{CL})$. Hence, we can successfully fit the experiments, as shown in Fig. 2(b) (dashed line) by posing $A = \kappa a$, $B = \kappa b$, and $C = c/\tau$ in which $\kappa = 1$ cm/ms and $\tau = 1$ ms restore physical dimensions, and $a = 0.177$, $b = 0.31$, $c = -0.015$ are nondimensional parameters. Based on this fit, we identify the characteristic length $\widehat{L_0}$ of the excitation wave by introducing a phenomenological constitutive relation in which the pacing CL acts as an internal variable,

$$\widehat{L_0} = \kappa \widehat{\mathrm{CV}}^{\alpha}\mathrm{CL}, \tag{3}$$

and $\widehat{\mathrm{CV}} = \mathrm{CV}/\kappa$ represents the experimental-based dimensionless dispersive conduction velocity restitution relationship. Equation (3) holds the notable limit of linear–nondispersive–wave propagation for $\alpha = 1$, shown in Fig. 3(a) [green (upper) dashed line]. We further remark that the quantity $\widehat{L_0}$ does not correspond to the concept of wavelength. Indeed, the characteristic length is based on an integral space-time operation and quantifies the response of the whole tissue at different pacing frequencies. From such a plot, it appears evident that the linear limit, also in the case of the chosen dispersive CV(CL) relation, is not able to reproduce the sought characteristic lengths L_0. Figure 4, in fact, shows linear and log-log plots of the characteristic length as a function of CV. In particular, Fig. 4(a) highlights the vertical saturation effect at high CV providing $\widehat{L_0}$ as independent of the pacing rate for physiological conditions. However, a horizontal asymptote appears at small CV greatly varying $\widehat{L_0}$ at fast critical pacings. The log-log plot in Fig. 4(b) further supports the power-law trend assumed for interpolating CV(CL) restitution curves.

We performed, then, a second fitting procedure to identify the values of α able to reproduce such a global and

synthetic length. Our analysis shows that both for the experiment (dashed blue) and model (dashed red), the exponent able to replicate the measured L_0 corresponds to $\alpha \simeq 1.5$. This particular value is in agreement with the fractional Laplacian operator exponent showed to replicate experimental dispersion of repolarization in human cardiac tissue [28,29] and that is based on a microscopic biophysics description of cardiac propagation. The result, by analogy in a homogenized micro-macro perspective, can be read as (i) a spatiotemporal generalization of scale invariance usually adopted in fractal geometry [30] and (ii) the fractional diffusion description of cell-cell coupling in cardiac electrophysiology [28,31,32].

Domain mapping for ventricular fibrillation. Upon this result, we analyze ventricular fibrillation both for the experimental preparations and the mathematical model. Fibrillation is an autoexcitatory regime (no external pacing) presenting multiple unstable spirals at the same time within the tissue (usually three for both experiments and simulations—see SM), and much shorter decay lengths [19]. Our analysis reveals that L_0 falls to an average value of 1.1 cm for the endocardial experimental data [see Fig. 3(a), red area (right)–squared symbol] supporting evidence that cardiac fibrillation is not a spatially random mechanism but a high-dimensional process characterized by a measurable degree of coherence [33–35]. Accordingly, numerical simulations confirm $L_0 \simeq 1.4$ cm only when a domain scaling procedure is applied [see Fig. 3(a), red area (right)–circle symbol]). Such a scaling methodology is necessary to reproduce *in silico* the spiral meandering observed in the experiments within a realistic tissue size. We solve such well-known problem as follows: (1) We simulate a sustained fibrillation scenario in a *nonphysical* squared domain with side length $\Delta = 20$ units where unit $=$ 1 cm; (2) we perform a downscaling of the domain size according to the fitted value of the exponent, $\alpha = 1.5$, defining the unit $= 0.37$ cm that leads to the physical domain size expected from the experiments, i.e., $\delta = \Delta^{1/\alpha} = 7.4$ cm; (3) we overimpose the irregular mask boundaries from the experiments; (4) we perform the spatiotemporal correlation analysis within the physical box of size 3×3 cm^2 (in agreement with the experimental case) and identify the sought decay length.

Discussions and perspectives. Physiological cardiac synchronization features are associated with long-range correlated dynamics corresponding to large spatial depolarization or repolarization states. Pathological behaviors, instead, are related to short-range coherent local states. In such a scenario, we address the interpretation of spatial correlation supporting both an augmented system's understanding and mathematical model predictivity. The physical meaning of such a value is regarded as the total length through which the activation wave must propagate to synchronize the whole organ as well as to restore the resting condition in a unified manner (full depolarization and repolarization phases consolidating additional information than the sole wavelength [36]). Besides, we characterize the transition of the excitation wave starting from normal rhythm (nonalternating), passing through a period-doubling bifurcation (concordant and discordant alternans), and ending with sustained ventricular fibrillation. To this end, we quantified the characteristic length transitions obtained during the pace-down stimulation protocol recorded for several experiments following the usual restitution procedure in cardiac electrophysiology [5]. We thus identify critical values of the decay length: $L_0 \sim 10$ cm at the onset of discordant alternans (CL ~ 200 ms), and $L_0 \leqslant 3$ cm at the onset of fibrillation (CL ~ 100 ms). On these pieces of evidence, we develop a unified criterium in terms of the characteristic length of the system, either L_0 or $\widehat{L_0}$, entailing, in a homogenized sense, feedback instabilities due to intra- and intercellular multiscale interactions. Accordingly, we incorporate our findings into a phenomenological constitutive law based on wave-front CV(CL) restitution properties. The advantage of our method over previous attempts to predict excitation adaptability, alternans, and arrhythmia onset [36,37] is due to incorporating spatiotemporal information in an integral and feedback sense, thus predicting cardiac instabilities. Our phenomenological theory indicates that a fractional exponent ($\alpha = 3/2$) best replicates the experimental decay lengths of the system during sustained pacing. Accordingly, we extrapolate this value to fibrillation scenarios by introducing a domain size mapping allowing us to reproduce the physical spatiotemporal features of the system without modifying any of the model parameters. Such theoretical reasoning, making use of nonlinear phenomenological laws, clearly suggests the need for a deeper understanding of cardiac tissue in terms of microstructural features and nonlocal diffusion operators [6,38–42], interscale coupling [43] and information flow [44,45], molecular diffusion [46], and spatiotemporal renormalization [47] to replicate and predict emerging phenomena in cardiac electrophysiology.

Acknowledgments. The authors acknowledge the support of the International Center for Relativistic Astrophysics Network (ICRANet), the Italian National Group for Mathematical Physics (GNFM-INdAM), the Visiting Professor Programme at Campus Bio-Medico University of Rome, and the National Science Foundation under Grant No. CNS-1446312.

[1] L. Glass, Nature (London) **410**, 277 (2001).
[2] Z. Qu, G. Hu, A. Garfinkel, and J. N. Weiss, Phys. Rep. **543**, 61 (2014).
[3] M. Scardigli, C. Crocini, C. Ferrantini, T. Gabbrielli, L. Silvestri, R. Coppini, C. Tesi, E. A. Rog-Zielinska, P. Kohl, E. Cerbai, C. Poggesi, F. S. Pavone, and L. Sacconi, Proc. Natl. Acad. Sci. USA **114**, 5737 (2017).
[4] M. R. Guevara, L. Glass, and A. Shrier, Science **214**, 1350 (1981).
[5] A. Gizzi, E. M. Cherry, G. R. F. Jr, S. Luther, S. Filippi, and F. H. Fenton, Front. Physiol. **4**, 71 (2013).
[6] A. Gizzi, A. Loppini, E. M. Cherry, C. Cherubini, F. H. Fenton, and S. Filippi, Physiol. Meas. **38**, 833 (2017).
[7] J. Han and G. K. Moe, Circ. Res. **14**, 44 (1964).

[8] F. L. Burton and S. M. Cobbe, Cardiovasc. Res. **50**, 10 (2001).
[9] F. H. Fenton, A. Gizzi, C. Cherubini, N. Pomella, and S. Filippi, Phys. Rev. E **87**, 042717 (2013).
[10] J. M. Pastore, S. D. Girouard, K. R. Lautira, F. G. Akar, and D. S. Rosenbaum, Circulation **99**, 1385 (1999).
[11] C. J. Wiggers, Am. Heart J. **20**, 399 (1940).
[12] V. Schulte-Frohlinde, Y. Ashkenazy, P. C. Ivanov, L. Glass, A. L. Goldberger, and H. E. Stanley, Phys. Rev. Lett. **87**, 068104 (2001).
[13] E. M. Cherry and F. H. Fenton, Am. J. Physiol.: Heart Circ. Physiol. **286**, H2332 (2004).
[14] S. Takagi, A. Pumir, D. Pazó, I. Efimov, V. Nikolski, and V. Krinsky, Phys. Rev. Lett. **93**, 058101 (2004).
[15] E. M. Cherry and F. H. Fenton, New J. Phys. **10**, 125016 (2008).
[16] I. V. Biktasheva, H. Dierckx, and V. N. Biktashev, Phys. Rev. Lett. **114**, 068302 (2015).
[17] J. Landaw, A. Garfinkel, J. N. Weiss, and Z. Qu, Phys. Rev. Lett. **118**, 138101 (2017).
[18] D. A. Egolf and H. S. Greenside, Nature (London) **369**, 129 (1994).
[19] P. V. Bayly, E. E. Johson, P. D. Wolf, H. S. Greenside, W. M. Smith, and R. E. Ideker, J. Cardiovasc. Electrophysiol. **4**, 533 (1993).
[20] Y. Ashkenazy, P. C. Ivanov, S. Havlin, C.-K. Peng, A. L. Goldberger, and H. E. Stanley, Phys. Rev. Lett. **86**, 1900 (2001).
[21] T. Quail, A. Shrier, and L. Glass, Phys. Rev. Lett. **113**, 158101 (2014).
[22] See Supplemental Material at http://link.aps.org/supplemental/10.1103/PhysRevE.100.020201 for more details of the numerical model adopted to perform simulations with respect to experimental analysis.
[23] F. H. Fenton and E. M. Cherry, Scholarpedia **3**, 1868 (2008).
[24] S. Mironov, J. Jalife, and E. G. Tolkacheva, Circulation **118**, 17 (2008).
[25] F. H. Fenton, E. M. Cherry, A. Karma, and W. J. Rappel, Chaos **15**, 013502 (2005).
[26] A. Barone, F. H. Fenton, and A. Veneziani, Chaos **27**, 093930 (2017).
[27] R. H. Clayton, O. Bernus, E. M. Cherry, H. Dierckx, F. H. Fenton, L. Mirabella, A. V. Panfilov, F. B. Sachse, G. Seemann, and H. Zhang, Prog. Biophys. Mol. Biol. **104**, 22 (2011).
[28] A. Bueno-Orovio, D. Kay, V. Grau, B. Rodriquez, and K. Burrage, J. R. Soc., Interface **11**, 20140352 (2014).
[29] N. Cusimano, A. Bueno-Orovio, I. Turner, and K. Burrage, PLoS One **10**, e0143938 (2015).
[30] A. L. Goldberger, L. A. Amaral, J. M. Hausdorff, P. C. Ivanov, C. K. Peng, and H. E. Stanley, Proc. Natl. Acad. Sci. USA **99**, 2466 (2002).
[31] A. Bueno-Orovio, D. Kay, and K. Burrage, BIT **54**, 937 (2014).
[32] A. Bueno-Orovio, I. Teh, J. E. Schneider, K. Burrage, and V. Grau, IEEE Trans. Med. Imag. **35**, 2200 (2016).
[33] A. L. Goldberger, V. Bhargava, B. J. West, and A. J. Mandell, Physica D **19**, 282 (1986).
[34] R. A. Gray, A. M. Pertsov, and J. Jalife, Nature (London) **392**, 75 (1998).
[35] M. Yashima, Y. H. Kim, S. Armin, T. J. Wu, Y. Miyauchi, W. J. Mandel, P. S. Chen, and H. S. Karagueuzian, Am. J. Physiol.: Heart Circ. Physiol. **284**, H249 (2003).
[36] G. D. K. Matthews, I. N. S. L. Guzadhur, A. A. Grace, and C. L.-H. Huang, J. Physiol. **591**, 4167 (2013).
[37] D. D. Chen, R. A. Gray, I. Uzelac, C. Herndon, and F. H. Fenton, Phys. Rev. Lett. **118**, 168101 (2017).
[38] D. E. Hurtado, S. Castro, and A. Gizzi, Comput. Methods Appl. Mech. Eng. **300**, 70 (2016).
[39] C. Cherubini, S. Filippi, A. Gizzi, and R. Ruiz-Baier, J. Theor. Biol. **430**, 221 (2017).
[40] N. Cusimano and L. Gerardo-Giorda, J. Comput. Phys. **362**, 409 (2018).
[41] A. Loppini, A. Gizzi, R. Ruiz-Baier, C. Cherubini, F. H. Fenton, and S. Filippi, Front. Physiol. **9**, 1714 (2018).
[42] P. Lenarda, A. Gizzi, and M. Paggi, Eur. J. Mech. A - Solids **72**, 374 (2018).
[43] S. H. Weinberg, Chaos **27**, 093908 (2017).
[44] H. Ashikaga and R. G. James, Chaos **28**, 075306 (2017).
[45] D. Sohn, K. Aronis, and H. Ashikaga, Comput. Biol. Med. **104**, 291 (2019).
[46] D. S. Novikov, J. H. Jensen, J. A. Helpern, and E. Fieremans, Proc. Natl. Acad. Sci. USA **111**, 5088 (2014).
[47] H. Ashikaga, F. Prieto-Castrillo, M. Kawakatsu, and N. Dehghani, Front. Phys. **6**, 30 (2018).